ACS NANO

Cite This: ACS Nano 2019, 13, 5451−5464

www.acsnano.org

ARTICLE

Nanoparticles to Knockdown Osteoporosis-Related Gene and Promote Osteogenic Marker Expression for Osteoporosis Treatment

Patricia Mora-Raimundo,[†] Daniel Lozano,[†,‡] Miguel Manzano,*[,†,‡] and María Vallet-Regí*[,†,‡]

[†]Chemistry in Pharmaceutical Sciences, School of Pharmacy. Universidad Complutense de Madrid, Spain. Instituto de Investigación Sanitaria Hospital 12 de Octubre i + 12, Plaza de Ramón y Cajal s/n, E-28040 Madrid, Spain

[‡]Networking Research Center on Bioengineering, Biomaterials and Nanomedicine (CIBER-BBN), E-28034 Madrid, Spain

Supporting Information

ABSTRACT: **Osteoporosis is the most common disease involving bone degeneration. Current clinical treatments are not able to offer a satisfying curative effect, so the development of effective treatments is desired. Gene silencing through siRNA delivery has gained great attention as a potential treatment in bone diseases. SOST gene inhibits the Wnt signaling pathway reducing osteoblast differentiation. Consequently, silencing SOST genes with a specific siRNA could be a potential option to treat osteoporosis. Generally, siRNAs have a very short half-life and poor transfection capacity, so an effective carrier is needed. In particular, mesoporous silica nanoparticles (MSNs) have attracted great attention for intracellular delivery of nucleic acids. We took advantage of their high loading capacity to further load the pores with osteostatin, an osteogenic peptide. In this study, we developed a system based on MSNs coated with poly(ethylenimine), which can effectively deliver SOST siRNA and osteostatin inside cells, with the consequent augmentation of osteogenic markers with a synergistic effect. This established the potential utility of MSNs to co-deliver both biomolecules to promote bone formation, this being a potential alternative to treat osteoporosis.**

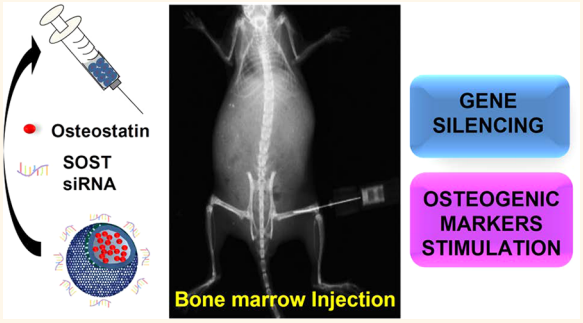

KEYWORDS: *mesoporous nanoparticles, gene silencing, osteoporosis, therapeutic co-delivery, osteogenic stimulation*

In the last few decades, the mean life expectancy has increased, which has consequently boosted the impact of skeletal diseases. In healthy adults, bone is continuously renewed by a coordinated process in which osteoclasts resorb old bone and osteoblasts synthesize and mineralize new bone matrix.[1] Imbalances in this physiological process, more-pronounced bone resorption, commonly produce a decreased bone mass and microarchitectural deterioration of bone tissue, named osteoporosis.[2,3]

The conventional treatment options of osteoporosis are limited to (1) anti-resorptive drugs that act mainly by suppressing osteoclast activity, preserving bone mass and increasing bone strength; and (2) anabolic agents that induce bone formation, effectively increasing bone mass and reversing bone deterioration.[4] However, current pharmacological therapy presents some limitations related to bioavailability issues and toxicity.[5] Thus, bisphosphonates, which are the most clinically used anti-resorptive therapeutic drugs, are poorly absorbed from the gastrointestinal tract.[6] Consequently, high doses are required, which leads to gastrointestinal problems.[7] Another commonly used antiresorptive drug is Denosumab (anti-receptor activator of nuclear factor κB ligand (RANKL) monoclonal antibody), which reduces bone resorption by decreasing osteoclast activation and differentiation. As a member of the tumor necrosis factor family, RANKL is also expressed on T lymphocytes; therefore, its inhibition could lead to impaired immunity.[8] However, parathyroid hormone (PTH), which was the first anabolic agent to be approved, stimulates osteoblast function by binding to a specific receptor and activating several signaling pathways.[9] Additionally, PTH therapy presents some disadvantages, such as the activation of bone resorption and the limited efficacy on nonvertebral fractures. These drawbacks justified the research of novel analogs exhibiting "pure" bone anabolism.[10] Different N-terminal PTH related protein (PTHrP) peptides such as PTHrP (1−36) or PTHrP (1−34) (abaloparatide) also bind to the PTH/PTHrP type 1 receptor as PTH. They activate the signal transduction with

Received: January 10, 2019
Accepted: May 9, 2019
Published: May 9, 2019

DOI: 10.1021/acsnano.9b00241
ACS Nano 2019, 13, 5451−5464

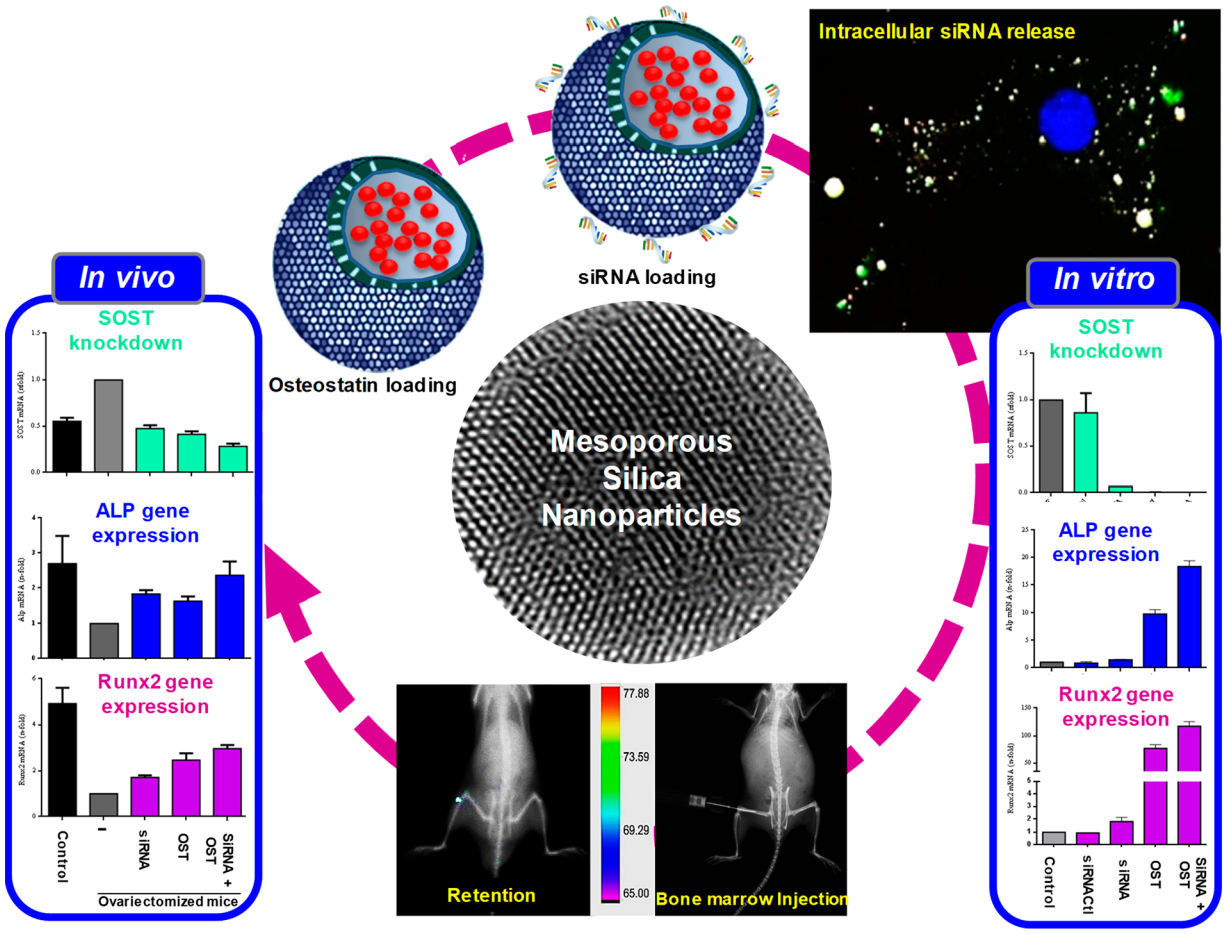

Figure 1. Schematic representation of the designed nanocarrier based on mesoporous silica nanoparticles loaded with osteostatin and siRNA to knockdown SOST and promote the expression of early markers of osteogenic differentiation both *in vitro* and *in vivo*.

equal potency as PTH but produce less activation of bone resorption.[9] The C-terminal fragment of PTHrP (107−111) (osteostatin) has been found to be an important osteoclast inhibitor while inducing osteogenic features *in vitro* and stimulating bone regeneration *in vivo*.[11−14] However, the intravenously administration of those peptides might be impeded by proteases, opsonization, and agglutination. Our group showed that it is possible to use bulk mesoporous ceramics or hidroxyapatites to deliver this peptide both *in vitro* and *in vivo*.[15−17] However, if intravenous delivery might be targeted, other vectors need to be developed. Consequently, as it has been stated above, all of these conventional osteoporotic drugs have a healing effect far from satisfactory, and their several side effects limit their further application.

Therapies based on gene expression modification have merged as potential alternative treatments to bone diseases. RNA interference is a natural cellular process that regulates gene expression. It enables the degradation of a specific mRNA (mRNA) and, therefore, knockdown-specific proteins.[18] According to this, RNAi-based therapies, in which genes that have been identified to down-regulate bone formation, could be targeted leading to an alternative treatment for osteoporosis.[19] In this sense, gene silencing through the delivery of small interfering RNA (siRNA) has gained great attention as a method to increase bone formation.[20−22] Wnt/β-catenin is a major signaling pathway that regulates bone development and remodeling.[23] This pathway is inhibited by the protein sclerostin and encoded by SOST gene. The inhibition of the Wnt/β-catenin signaling pathway decreases bone formation by reducing osteoblast differentiation.[24−26] For this reason, silencing SOST gene using siRNAs could be an effective way of reducing sclerostin expression and, therefore, increasing bone formation and potentially treating osteoporosis.

Generally, siRNAs are well-known for their very short half-life and their poor penetration capacity through cell membranes.[20,21] These unresolved issues have induced the use of nanocarriers to protect and deliver siRNAs. Among them, different polymeric nanoparticles, including liposomes[27,28] or cationic-polymeric nanoparticles[29,30] have been proposed as siRNA nanocarriers. In this sense, poly(ethylenimine)-siRNA complexes have been investigated for siRNA delivery, although their high cytotoxicity has compromised their use.[31]

Mesoporous silica nanoparticles (MSNs) have attracted research interest in biomedicine due to their great properties for drug delivery, such as large surface area, high loading capacity, and biocompatibility.[32−35] It could also be highlighted that their surface could be chemically modified with different moieties to provide MSNs with different capabilities. Normally, surface modifications are carried out to improve the targeting ability of nanoparticles[36,37] or to design stimuli-responsive nanocarriers.[38,39] In this sense, MSNs can be functionalized with cationic polymers such as poly(ethylenimine) (PEI) to transport siRNAs and achieve a better uptake by cells.[40,41] In fact, MSNs covered with PEI have been reported to be biocompatible, showing much less

DOI: 10.1021/acsnano.9b00241
ACS Nano 2019, 13, 5451−5464

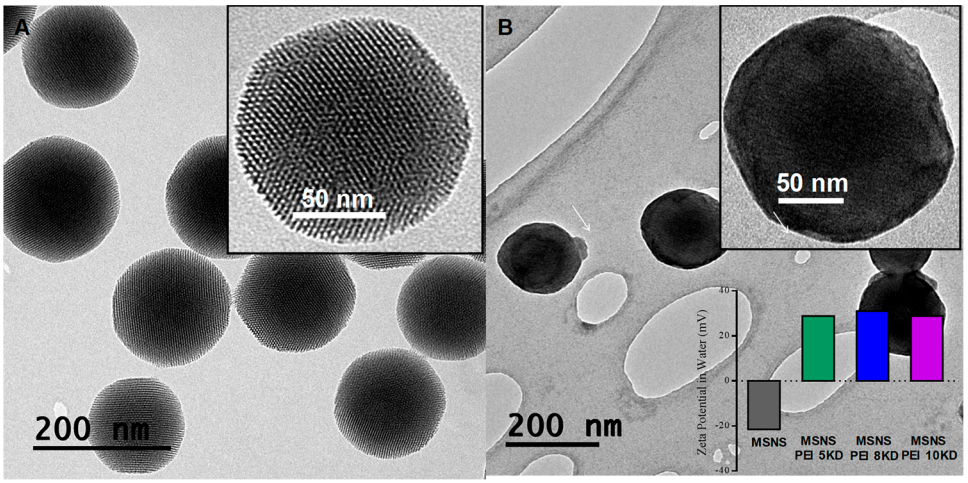

Figure 2. PEI grafting to MSNs surface. TEM micrographs of the nanoparticles (A) before and (B) after coating with 5 kDa PEI polymer. The ζ potential before and after coating with 5, 8, and 10 kDa PEI polymer (bottom right corner inset).

cytotoxicity to cells than the PEI-siRNA complexes mentioned above.[40]

In this work, we have engineered a system based on MSNs coated with PEI that can effectively bind and deliver SOST siRNA, preserving its knockdown capability and increasing bone formation (Figure 1). We took advantage of the high loading capacity of MSNs to further loading the pores with osteostatin, which has been observed to stimulate osteoblastic cell growth and differentiation.[42] Thus, this dual therapy is expected to boost bone formation being a potential alternative to the current treatments for osteoporosis.

RESULTS AND DISCUSSION

MSNs@PEI and Effective Loading and Delivering of SOST siRNA inside Cells. Mesoporous silica nanoparticles with diameter of *ca.* 150 nm and mesopores of 2 nm were synthesized following a modification of the Stöber method.[43] (See the Methods section for details of MSNs synthesis, functionalization, and characterization.) The external surface of the nanoparticles was functionalized with phosphonate groups, providing the strong negative charge to the nanoparticles surface needed to coat them afterwards with the cationic polymer. The PEI grafting to MSNs surface was verified by different characterization techniques as it is described below. The PEI coating was confirmed through the phosphotungstic acid stained-layer covering the surface of PEI functionalized nanoparticles, which was not present on the plain as it can be appreciated by transmission electron microscopy (TEM). TEM also showed that the nanoparticles were spherical and monodispersed (Figure 2A).

MSNs presented the characteristic zeta potential of −21.5 mV at pH = 7, which was shifted to positive and 31 mV at pH = 7 after PEI coating (Figure 2B). These data confirm that the external surface of the particles was successfully grafted with the polymer (more details of the characterization can be found in the Supporting Information).

The aim of covering the surface of MSNs with PEI was to provide them with the ability to bind siRNA. However, depending on the molecular weight employed, PEI could damage the cell membrane, mitochondria, and lysosomes.[44,45] Therefore, optimization of PEI coating was the first task to accomplish in this work using different molecular weights (5, 8, and 10 kDa). Their capacity of binding to siRNA versus reduction of toxicity was evaluated using a fluorescent siRNA-analog (siGLO Green Transfection Indicator).

In vitro cell viability of MSNs coated with PEI (MSNs@PEI) was evaluated by incubating the nanoparticles at different concentrations with mouse embryonic fibroblast (MEF) cells for 2 h. Then, the cell viability was measured after 48 h of incubation, and it was found that MSNs@PEI of 10 kDa reduced the cellular viability at concentrations >100 μg/mL (Figure 3A). In contrast, nanoparticles coated with 8 or 5 kDa PEI showed no toxic effects at concentrations as high as 200 μg/mL. It should be noted that bare nanoparticles without PEI coating were nontoxic for MEF cells at concentrations as high as 200 μg/mL. Therefore, MSNs@PEI of 10 kDa were refused due to their toxicity, and we focused on MSNs@PEI of 5 kDa.

The siRNA delivery from MSNs@PEI was initially determined by the binding capacity of the polymeric coating towards the nucleic acid. The highest amount of siRNA that could be bound to MSNs@PEI was determined by agarose gel electrophoresis. In particular, different amounts of MSNs@PEI ranging from 0.8 to 6.4 μg (using PEI with different molecular weights) were dispersed with 0.1 μg of siRNA in aqueous solution to obtain particle-to-nucleic acid ratios (N/P) of 8–64. N/P is a mass ratio in which N and P, respectively, correspond to the mass of positive (nitrogen (MSNs@PEI)) and negative (phosphonate (siGLO)) charges (Figure 3B). The ratio results from dividing the μg of nanoparticles between the μg of siRNA. One channel was filled just with siGLO as control (ϕ). Then, these dispersions with different nanoparticle to siRNA (N/P) ratios were electrophoresed. Only uncomplexed siGLO was able to migrate to the positive electrode and, therefore, be observed on the gel. Thus, when the band generated by siGLO is no longer visible means that all the nucleic acid has been complexed with the added nanoparticles, and that would be the optimal concentration of nanoparticles needed to complex the siGLO present. The results observed in Figure 3b indicated that all siGLO was bound to the nanoparticles at a N/P ratio of >16 (for PEI 5 kDa) and >32 (for PEI 8 and 10 kDa). Thus, 16 μg of MSNs@PEI 5 kDa were needed to load 1 μg of siGLO and 32 μg of the MSNs@PEI 8 and 10 kDa. Consequently, the siRNA loading capacity of the nanoparticles was found to be *ca.* 5 wt %. Taking into consideration that the amount of siRNA recommended by the manufacturer to achieve a proper

DOI: 10.1021/acsnano.9b00241
ACS Nano 2019, 13, 5451−5464

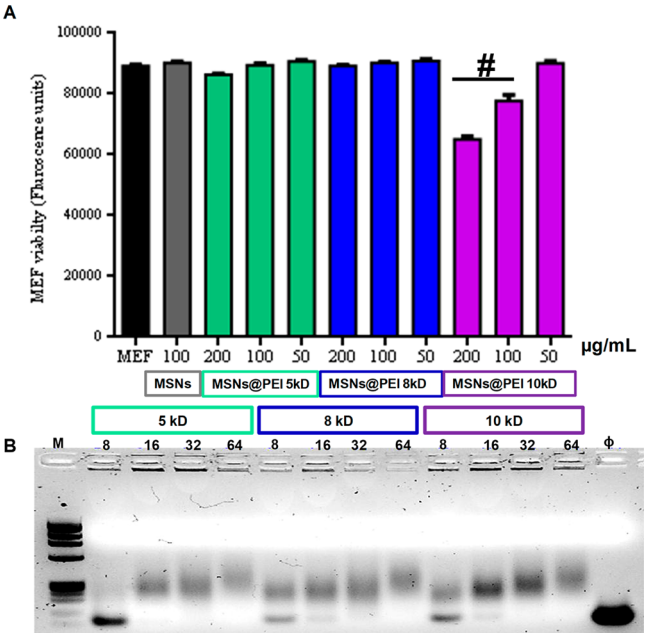

Figure 3. Effective SOST siRNA model molecule binding to MSNs@PEI and cell viability in mouse embryonic fibroblast (MEF) cells. (A) MEF cell viability (measured by Alamar Blue) in contact with different concentrations of MSNs@PEI nanoparticles at 48 h of cell culture. Data are mean ± SEM of three independent experiments performed in triplicate. Pound signs indicate $p < 0.01$ *vs* MSN, MSNs@PEI 5kD, and MSNs@PEI 8kD. (B) Agarose gel electrophoresis of MSNs@PEI and complexed siGLO siRNA in different nanoparticle to nucleic acid (N/P) ratios. M: molecular weight marker. The ϕ lane contains only siRNA. After the loading of osteostatin, the N/P ratio and the electrophoretic mobility did not change. The data showed that all siRNA was bound when the N-to-P ratio was over 16 in MSNs@PEI 5 kDa, and over 32 in the case of PEI 8 kDa and PEI 10 kDa.

knockdown effect was around 0.5−1 μM, it means that final concentration should be between 6.65 and 13.3 μg/mL. Thus, taking into account the ratio obtained (16 N/P ratio), we can aproximate that the nanoparticle concentration should be between 106 and 213 μg/mL, which is within the nontoxicity window for 5 kDa PEI. Then, although the loading capacity of the nanoparticles could be considered low, it was found to be good enough to transport the efficient amount of siRNA needed for an effective knockdown.

Consequently, the 5 kDa PEI resulted on the lowest cell toxicity of MSNs@PEI while maintaining the effective siRNA bind and delivery ability. Based on these results, the 5 kDa PEI was selected and further used for the next steps in our research. It is worth mentioning that the siRNA presence in the PEI mesh remained the cell viability unchanged (Figure S2).

The next step consisted on the evaluation of the cellular uptake of the MSNs@PEI through flow cytometry (Figure 4A) and confocal laser scanning microscopy (Figures 4B and 5). For the flow cytometry assay, FITC labeled nanoparticles (F-MSNs) coated with PEI and bound with siGLO were used. After coating the MSNs with PEI, the nanoparticle uptake significantly increased, which could be ascribed to the drastic change on the surface charge previously mentioned, from negative (MSNs) to positive (MSNs@PEI). This is in agreement with the literature because it is easier for the surface membrane (negative) to endocyte the positively charged nanoparticles (Figure 4A).[44] After the binding of the siGLO to the nanoparticles, the amount of nanoparticles internalized was approximately the same as expected, but the fluorescence intensity doubled, confirming that siGLO was inside the cells being the responsible of the fluorescence intensity increase.

For the microscopy assay, rhodamine B-labeled nanoparticles coated with PEI and bound with siGLO were used. The MSNs (red) and siGLO (green) co-localize in the cell (yellow), proving that the nucleic acid was attached to the PEI mesh at the initial stage of the experiment (Figure 4B).

The Rh-MSNs@PEI-siGLO were added to the cells and after 2 h, the media, including the non-internalized nanoparticles, were removed and refreshed. At that moment (0 h), green and red fluorescence co-localize, while after 48 h, the green fluorescence started to spread, turning green the cytoplasm, which could be ascribed to the siGLO being released from the Rh-MSNs@PEI (Figure 5).

The release kinetics of the MSN@PEI carrier was evaluated using siGLO as a siRNA model. Loaded nanoparticles were suspended in phosphate-buffered saline (PBS) and placed on a Transwell permeable support. At every time point studied, the amount of cargo released in the solution outside the transwell was determined by fluorescence. Figure S3 shows the release profile of siGLO from MSNs@PEI. At the beginning, only a small amount of the cargo was released (around 20% of the cargo after 24 h), possibly due to the strong interactions between PEI and siRNA.[30] However, over 80% of the cargo was released after 48 h as a consequence of the reduction of the electrostatic interaction between siGLO and the cationic mesh. This release delay would provide the system with the necessary time to arrive to the target area (osteoporotic bone) before releasing the cargo, providing the protection that siRNA needs around system circulation.

***In Vitro* Model for SOST Expression.** To demonstrate that the designed system could effectively knockdown the SOST gene *in vitro*, it was necessary to have a cell line that expressed this gene. In particular, it has been reported that MEFs generate detectable levels of SOST expression.[28] Thus, we cultured MEFs for 3 weeks observing increased levels of SOST expression detectable after 3 days, which were increased up to 20-fold after 14 days (Figure 6A). It was also observed that as SOST mRNA levels lessened, the expression of two osteoblastic differentiation markers, Runx2 and Alp, increased (Figures 6B,C).

As mentioned above, SOST gene is involved in different developmental processes, particularly, inhibits osteoblastic activity and differentiation, therefore modulates bone formation. Then, when cells differentiate, SOST expression falls and decreases to lower values, instead, different genes like Runx2 or Alp, known as osteogenic markers, increased their expression. The results obtained by real-time PCR are in agreement with this statement.

In consequence, MEFs provides an *in vitro* system in which SOST is greatly expressed after 2 weeks of incubation without the necessity to expose the cells to any osteogenic inductors. This system would permit us to study the SOST knockdown efficiency by the specific siRNA. In addition, the modified expression of osteogenic markers as well as SOST gene in MEF cells permits its use to evaluate the impact of SOST knockdown on bone osteogenic marker genes.

Silencing Capability of MSNs@PEI-siRNA. First, it was necessary to evaluate the free SiRNA capacity to *in vitro* knockdown SOST gene in MEF model. The transfection of

DOI: 10.1021/acsnano.9b00241
ACS Nano 2019, 13, 5451−5464

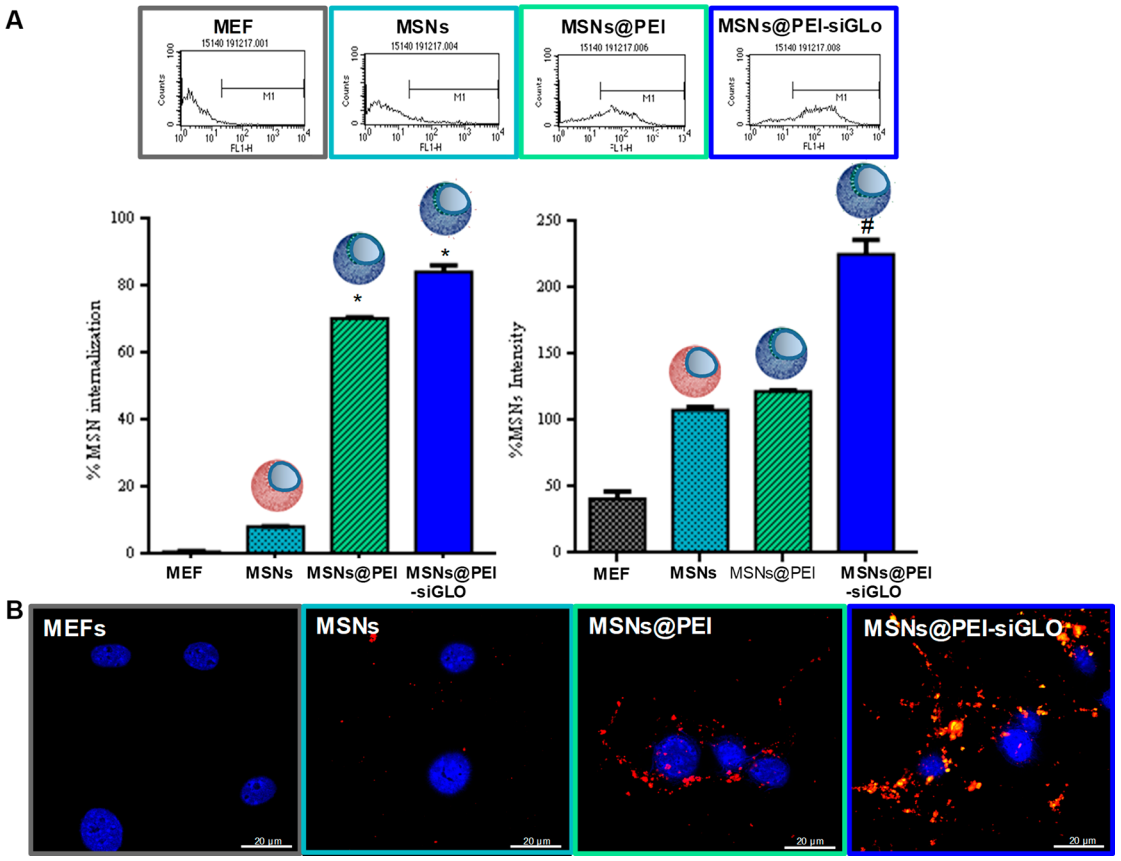

Figure 4. MSNs@PEI-siGLO uptake by mouse embryonic fibroblast (MEF) cells by flow cytometry and fluorescence microscopy. (A) Cellular uptake of different fluorescein-labeled MSNs, MSNs@PEI, and MSNs@PEI-siGLO was measured by flow cytometry at 2 h of internalization in MEF cells. Representative flow cytometry images are shown on the top. Data are mean ± SEM of three independent experiments performed in triplicate. Asterisks indicate $p < 0.03$ *vs* MSN; pound signs indicate $p < 0.01$ *vs* MSN and MSNs@PEI. (B) Representative confocal laser scanning microscopy images of MEF cells incubated with Rhodamine-B-labeled MSNs, MSNs@PEI, and MSNs@PEI-siGLO nanoparticles at 2 h of internalization. Blue fluorescence (nuclei), red fluorescence (Rh-MSNs@PEI), and green fluorescence (siGLO).

SOST siRNA to MEF cells was evaluated after 14 days of incubation in Dulbecco's modified Eagle medium (DMEM). That period of time was selected after the previous experiment, in which the maximum expression of SOST in MEF cells was observed after 14 days of culture. SiRNA transfection was promoted using Accell siRNA delivery media (free from BSA, which inhibit the transfection of free Accell siRNA). Quantitative reverse transcription polymerase chain reaction (qRT-PCR) was used to evaluate SOST expression after 2 h of transfection at day 14 of cell culture. A pair of controls were used to optimize the experiment: a negative control siRNA (SiCtl) ("non-targeting control", which targets a site that is absent in human, mouse, and rat genomes), as well as positive control (PosControl) ("GAPD control", which targets GAPDH, a gene common between human, mouse, and rat). SiCtl is necessary to verify that the silencing resulted from a sequence-specific process, and it is not due to a nonspecific effect. In contrast, PosControl targets a housekeeping gene, which means that the target gene is expressed in all cell types at a level that does not fluctuate with cell cycle. In this sense, PosControl would verify the efficiency of siRNA delivery into cells. It was also used an untreated control (MEF or MSNs@PEI MEF) to determine a baseline of target gene level. After evaluation of the gene expression levels (Figure S4), it was found that when treating the cells with the SiCtl, SOST expression was very similar to the untreated control (MEF). Instead, after applying the PosControl, SOST expression decreased to significantly lower levels, confirming that siRNA transfection was carried out successfully. The data obtained showed that the expression of SOST decreased notably (*ca.* 98%) after treatment with SOST siRNA, verifying its functionality and the utility of the *in vitro* model to assess afterwards the capability of MSNs@PEI to transfect siRNA into cells.

After confirming the siRNA activity, we have to take into account that in a real *in vivo* scenario, siRNA cannot just be injected into the bloodstream because it would be degraded, so a nanocarrier was designed for delivering the siRNA. It was necessary to verify that siRNA knockdown capability was maintained after being bound and released from MSNs@PEI. The efficacy of SOST siRNA delivered by MSNs@PEI was evaluated in MEFs. In this case, the MSNs would be the transfection vector, and then it was not necessary to use the Accell siRNA delivery media; hence, DMEM was used instead. At day 14 of culture, 600 μL of a 115 μg/mL MSNs@PEI dispersion bound with 15 μL of 20 μM siRNA were added to the cells, and after 2 h, the media were refreshed. Considering the amount of siRNA bound to the nanoparticles as well as the nanoparticles internalized inside the cells, we could approximate the amount of siRNA delivered to the cells, assuming that all the siRNA loaded would be released. A total of 600 μL of a 115 μg/mL MSNs@PEI dispersion bound with 15 μL of

DOI: 10.1021/acsnano.9b00241
ACS Nano 2019, 13, 5451−5464

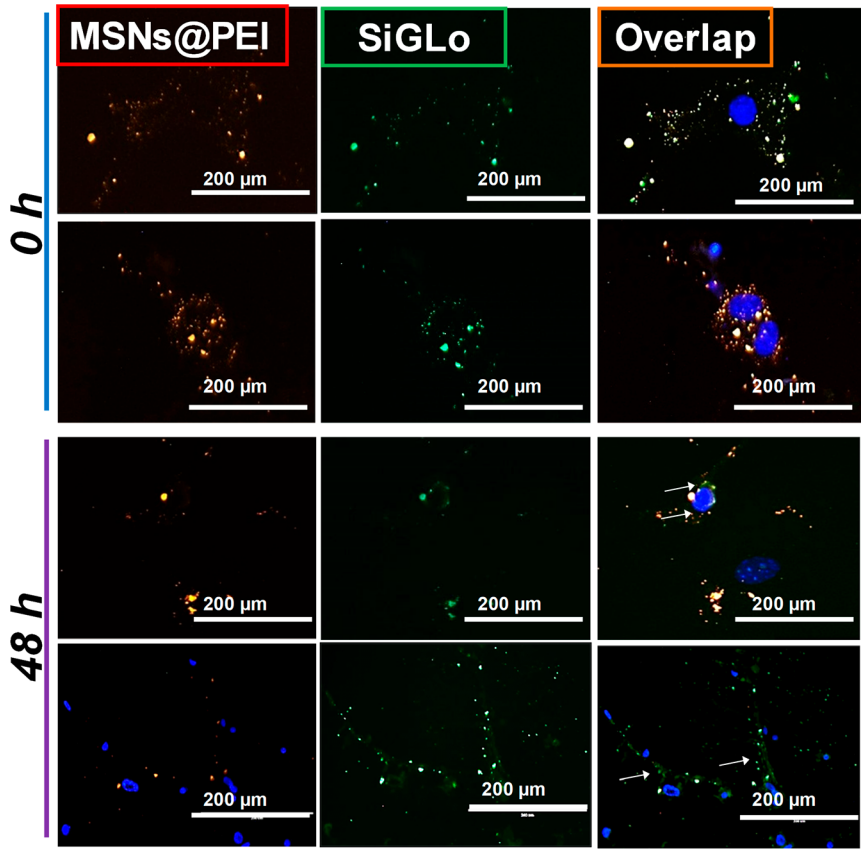

Figure 5. SiGLO release from MSNs@PEI in MEF cells. Representative fluorescence microscopy images of MEF cells incubated 2 h with MSNs@PEI nanoparticles with siGLO at 0 and 48 h after nanoparticle incubation. Blue fluorescence (nuclei), red fluorescence (MSNs@PEI), and green fluorescence (siGLO). Arrows denote the siGLO released.

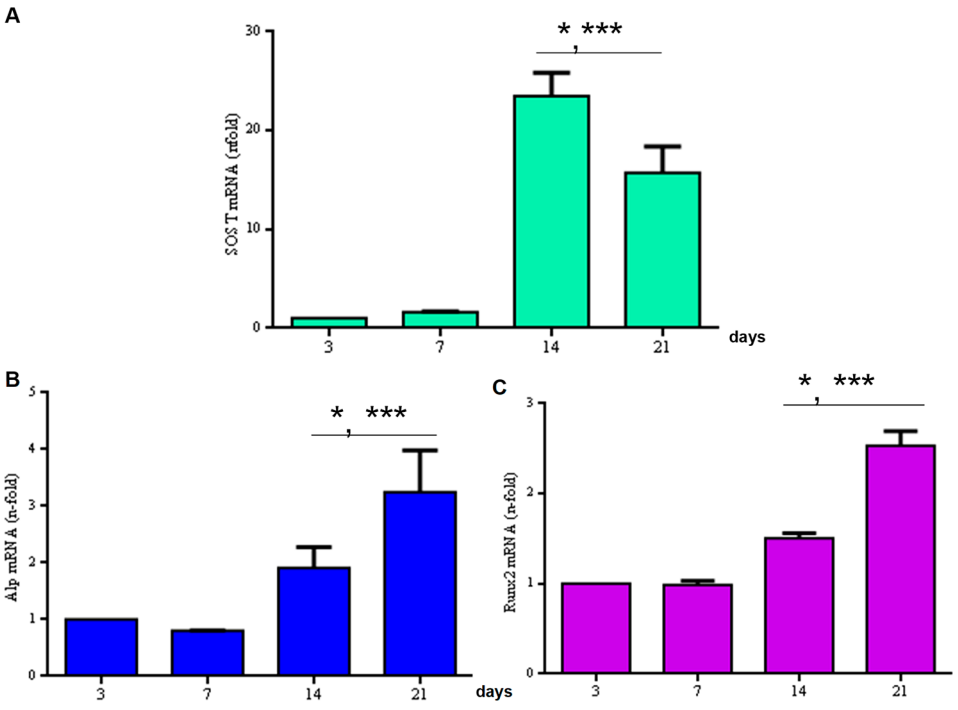

Figure 6. Changes in SOST mRNA levels and Runx2 and Alp bone osteogenic markers in MEF cells. (A) SOST, (B) Alp, and (C) Runx2 gene expression (measured by real-time PCR) in MEF cells at different times. Data are mean ± SEM of three independent experiments performed in triplicate. Single asterisks indicate $p < 0.01$ *vs* 3 days; triple asterisks indicate $p < 0.001$ *vs* 3 and 7 days.

DOI: 10.1021/acsnano.9b00241
ACS Nano 2019, 13, 5451−5464

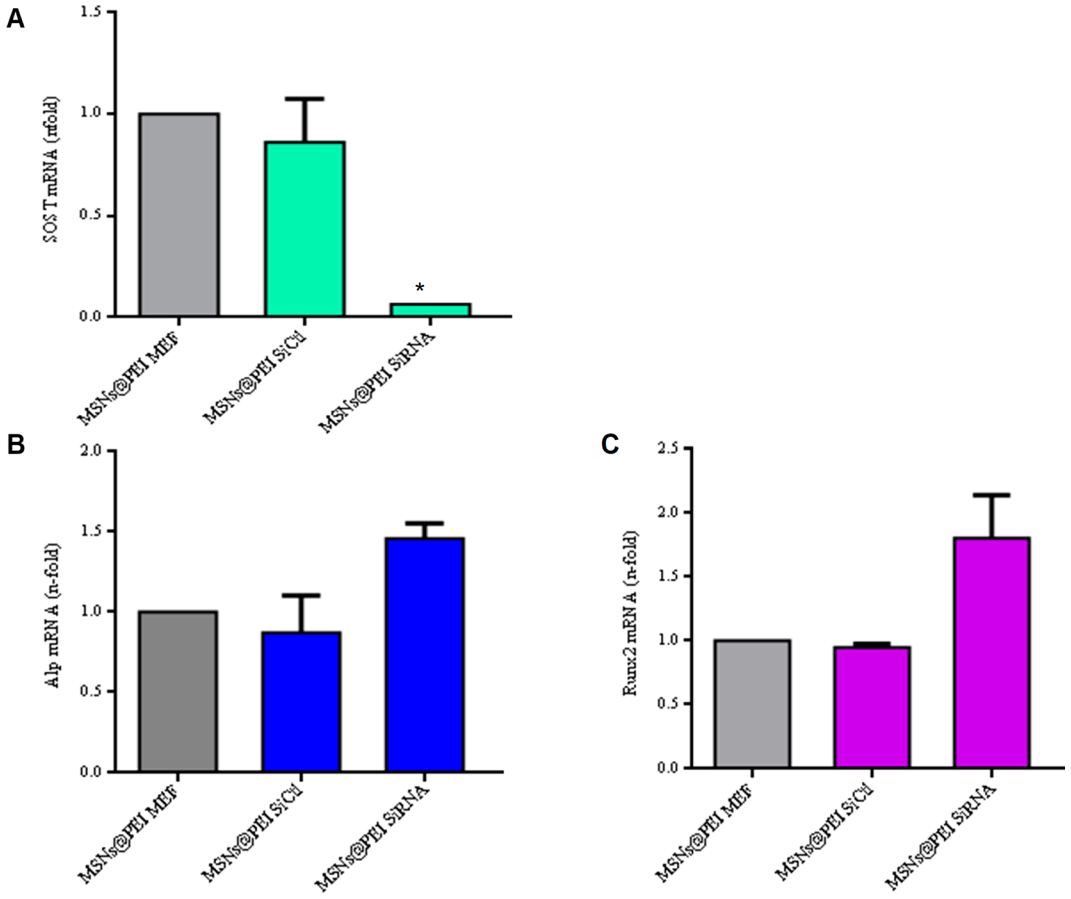

Figure 7. SOST, Runx2, and ALP gene expression in the presence of SiRNA-Sost bound to MSNs@PEI in MEF cells. (A) SOST mRNA expression (measured by real-time PCR) in MEF cells at 14 days of cell culture. (B) Alp and (C) Runx2 mRNA expression (measured by real-time PCR) in MEF cells at 14 days of cell culture. A negative-control siRNA (SiCtl) was used. MSNs@PEI nanoparticles bound to NeControl (MSNs@PEI SiCtl). Data are mean ± SEM of three independent experiments performed in triplicate. Asterisks indicate $p < 0.01$ *vs* MSNs@PEI MEF control cells.

20 μM of siRNA was added to cells, *i.e.* 70 μg of nanoparticles were loaded with 4 μg of siRNA. The 80% of the loaded nanocarriers were internalized, which means that, 56 μg of nanoparticles were taken up, and 3.2 μg of siRNA were released into cells.

Then, after 48 h, SOST-mRNA was measured using qRT-PCR. MEFs transfected with SOST siRNA presented a significant reduced expression of SOST relative to NeControl (*ca.* 95%) as well as MSNs@PEI control (Figure 7A), which was quite similar to the one obtained before with the Accell siRNA transfected with the Accell siRNA delivery media. Osteogenic markers gene levels (Runx2 and Alp) were also measured to determine the impact of SOST down-regulation (Figure 7B,C). Because SOST is a gene involved in cell-differentiation inhibition, its knockdown is expected to increase the expression of these osteogenic markers. The data showed, as it was proposed above, that when SOST was knocked down, the expression of the osteogenic markers increased, being correlated with a possibly increased cell differentiation in a complex environment such as osteopororotic bone. The expression of Runx2 increased up to 2-fold and Alp up to 1.5-fold after siRNA transfection compare to MEF cells expression (Figure 7B,C). The increment in bone osteogenic markers expression was slight; thus, the next step was to evaluate the coadministration with other anabolic agent to determine if an additive effect could be achieved.

Co-delivery of siRNA and Osteostatin to Cells and Its Effect in Osteogenic Marker Expression. Even though osteostatin has been shown to be effective at inducing osteoblast differentiation *in vitro* (even in the sub-nanometer range)[11−14] and increasing bone regeneration *in vivo*,[15−17] its use in combination with siRNAs has never been reported. As it has been mentioned above, MSNs could be used to explore that possible synergistic effect. For this reason, we designed a dual release system in which osteostatin would be loaded in the mesopores, and the therapeutic siRNA would be bound to the PEI network. In this sense, the system will be able to transport and release both molecules at the target destination, where the effect of their dual release would be evaluated.

First, it was necessary to test whether the PEI coating affects the osteostatin release from the MSNs. Osteostatin was loaded in the mesopores of the MSNs by immersing the nanoparticles in a solution of osteostatin overnight, and then the nanoparticles were coated with PEI. Afterwards, a release experiment was carried out, and the amount of osteostatin released was measured by fluorescence (Figure 8). Osteostatin release data showed in Figure 8 can be fitted to a first-order kinetic model, with a typical release profile from mesoporous materials (eq 1):[39]

$$Y = A(1 - e^{-kt}) \quad (1)$$

DOI: 10.1021/acsnano.9b00241
ACS Nano 2019, 13, 5451−5464

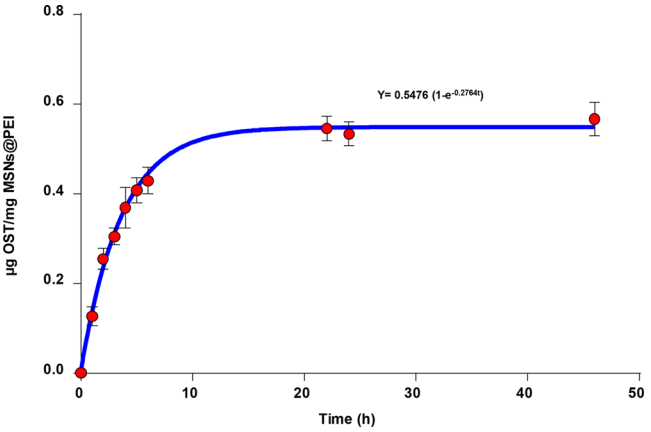

Figure 8. Time-dependent osteostatin (OST) release from MSNs@PEI in PBS at pH 7.4, simulating the physiological fluids. Nanoparticles were loaded with OST and afterwards coated with PEI (OST-MSNs@PEI). Points to trace the curves are the means of three independent measurements per time period.

The equation parameters could be described as Y being the amount of osteostatin released (microgram of osteostatin per milligram of MSNs@PEI) at time t (h), with A being the maximum amount of osteostatin released (in micrograms of osteostatin per milligram of MSNs@PEI), and with k being the release rate constant. The release data showed that MSNs loaded with osteostatin and coated with PEI (OST-MSNs@PEI) released osteostatin in a time-dependent manner, reaching values of 0.5476 micrograms of osteostatin per milligram of MSNs@PEI. Thus, despite PEI coating, which it is not acting as a physical barrier impeding the osteostatin release, the MSNs were able to release the cargo, so MSNs@PEI could be used to transport and deliver osteostatin. Osteostatin delivery from other mesoporous matrices, such as SBA15, has been previously explored *in vivo*, conferring osteoinductive features thanks to the peptide delivery. In fact, despite the non-controlled delivery of osteostatin, no clinical alterations were observed.[15]

After testing of the osteostatin and siRNA release separately, both components were integrated into a multifunctional system capable of release both biomolecules inside cells.

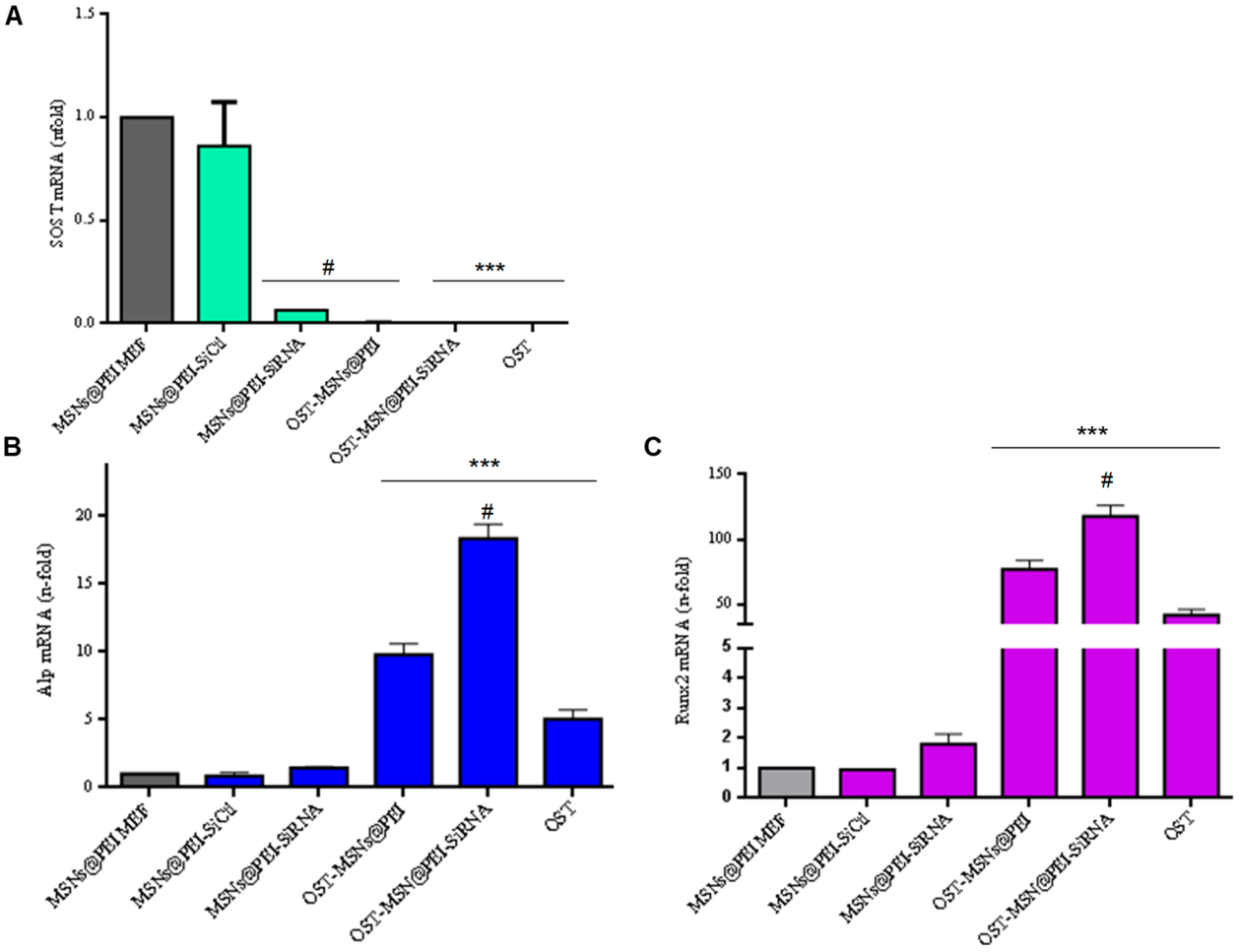

Figure 9. (A) SOST, (B) Alp, and (C) Runx2bone osteogenic markers gene expression in the presence of SiRNA-SOST bound to MSNs@PEI in mouse embryonic fibroblast (MEF) cells in the presence or absence of osteostatin (OST). SOST mRNA expression (measured by real-time PCR) in MEF cells at 14 days of cell culture and Alp and Runx2 mRNA expression (measured by real-time PCR) in MEF cells at 14 days of cell culture. To optimize the experiment, one control was used: a negative control siRNA (SiCtl) ("non-targeting control", which targets a site that is absent in human, mouse, and rat genomes); MSNs@PEI nanoparticles were bound to SiCtl (MSNs@PEI SiCtl). Data are mean ± SEM of three independent experiments performed in triplicate. Triple asterisks indicate $p < 0.001$ *vs* MSNs@PEI MEF; pound signs indicate $p < 0.05$ *vs* OST-MSNs@PEI and MSNs@PEI-SiRNA.

DOI: 10.1021/acsnano.9b00241
ACS Nano 2019, 13, 5451−5464

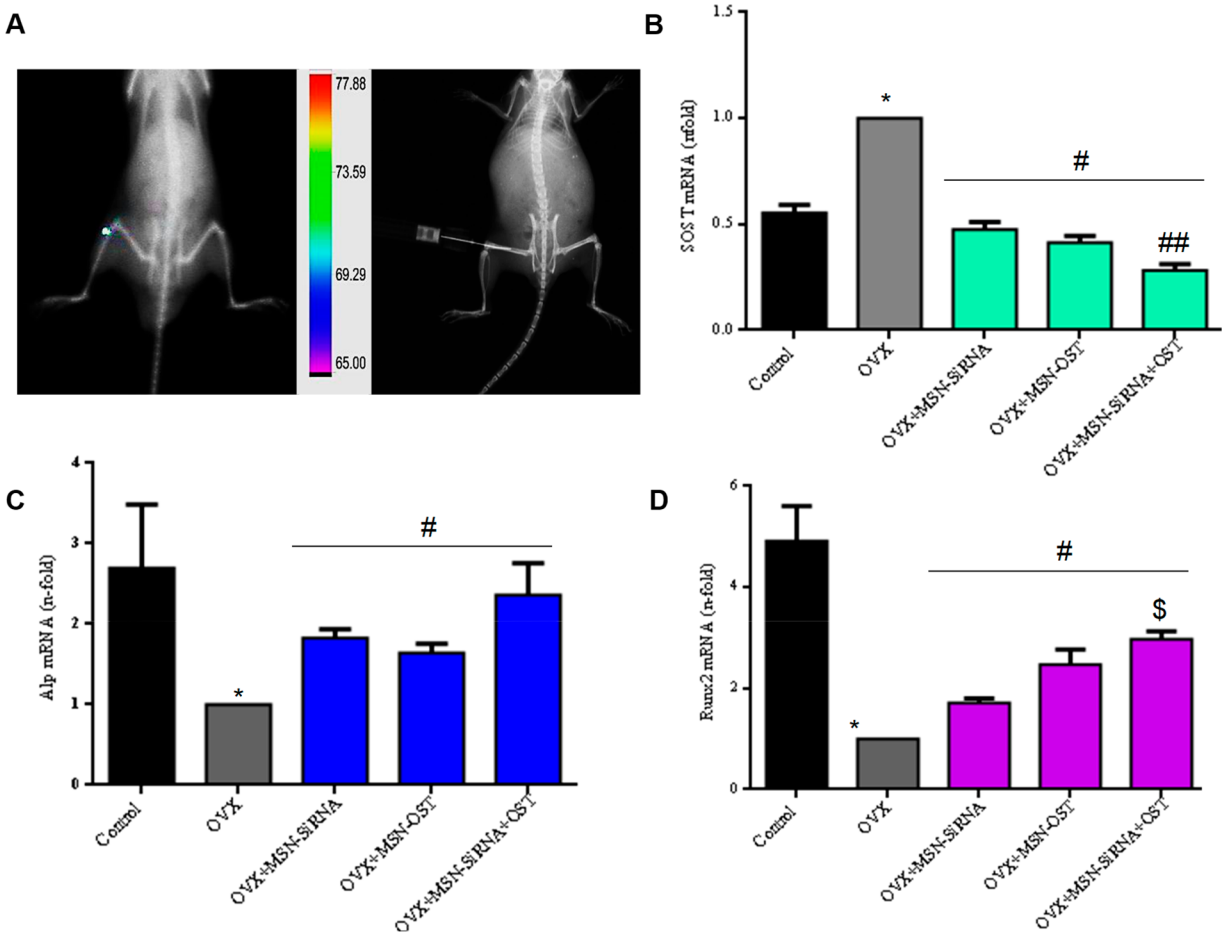

Figure 10. ***In vivo*** **injection of OST-MSNs@PEI-siRNA. SOST, Alp, and Runx2 bone osteogenic markers gene expression in the presence of SiRNA-SOST bound to MSNs@PEI in ovariectomized mice (OVX) in the presence or absence of osteostatin. (A) Femur bone-marrow injection in ovariectomized female mice and cyanine-7 labeled nanoparticles accumulation. (B) SOST mRNA expression (measured by real-time PCR) in femur bone. (C) Alp and (D) Runx2 mRNA expression (measured by real-time PCR) in femur bone. To optimize the experiment, one control was used: a negative control siRNA (SiCtl) ("non-targeting control", which targets an absent site in human, mouse, and rat genomes) and MSNs@PEI nanoparticles bound to SiCtl (MSNs@PEI SiCtl). Data are mean ± SEM of three independent experiments performed in triplicate. Triple asterisks indicate $p < 0.001$** ***vs*** **MSNs@PEI; pound signs indicate $p < 0.05$** ***vs*** **OST-MSNs@PEI and MSNs@PEI-SiRNA.**

First, osteostatin was loaded into the mesopores as described above. Then, the PEI coating was accomplished, and siRNA was bound, leading to the final system (OST-MSNs@PEI-siRNA). At day 14 of MEF cell culturing, the complete system was added to the cells following the same procedure described above. After 48 h, SOST-mRNA, Runx2 and Alp expression were measured (Figure 9). The results showed that SOST was effectively knocked down either by the SOST-siRNA release or the osteostatin release and, more efficiently, by the delivery of both molecules (Figure 9A). Furthermore, Alp expression rose up to 17-fold when OST-MSNs@PEI-siRNA were administrated (Figure 9B). Besides, Runx2 expression notably increased up to 110-fold when osteostatin and SOST siRNA were released together by the nanoparticles (Figure 9C). The results obtained with the administration of the nanocarrier loaded just with SOST siRNA (MSNs@PEI-siRNA) or only with osteostatin (OST-MSNs@PEI) were also measured and compared with those obtained with the nanocarrier loaded with both. The data showed that the coadministration of both biomolecules at the same time, compared with the administration of the biomolecules separately, increased the expression of both osteogenic markers to notably high levels, being a combined effect between osteostatin and siRNA. It was also measured the effect of one pulse of free osteostatin at the same concentration as the one achieved by the nanoparticles (7×10^{-7} M). It is true that in both cases (Runx2 and Alp), the gene expression levels rose up signaly higher when the osteostatin is released from the nanoparticles than when is added on its free form. This fact has been noticed before, producing higher effects in mineralization the continuous release of free osteostatin from a mesoporous biomaterial than one pulse of osteostatin at the beginning of the experiment.[17] The reasons that could support this theory are, first, that from the osteogenic perspective, a controlled and sustained released of osteostatin for longer time is more effective than a punctual administration of higher doses of osteostatin. Second, it has also been reported that, the mere presence of silica would increase the expression of different osteogenic markers as well as increase the proliferation of osteoblast.[46] In addition, the MSNs could also protect the peptide from degradation, being gradually released in perfect conditions. So, unlike just one pulse of osteostatin at the beginning of the experiment, which would be progressively degraded, the release from MSNs would keep a uniform concentration of active osteostatin for

DOI: 10.1021/acsnano.9b00241
ACS Nano 2019, 13, 5451−5464

longer time, being that the effect in this sense is more noticeable. Therefore, the delivery of osteostatin from our system improves osteostatin effects in osteogenic marker expression.

***In Vivo* Evaluation of siRNA and OST Co-delivery and Their Implications on Gene Expression.** After the successful *in vitro* validation of the system, the next step was the *in vivo* evaluation in a reduced bone mass model. It has been used ovariectomized C57/BL6 female mice with a decreased femoral bone mineral density compared to non-ovariectomized (62.98 ± 0.28 mg/cm^2 *versus* 66.56 ± 0.47 mg/cm^2; $p < 0.001$) as previously described.[47] First, 50 μL of the complete nanocarrier (OST-MSNs@PEI-siRNA) dispersion (0.8 mg/mL) were injected in the femur bone marrow of ovariectomized mice (Figure 10A). Even-higher concentrations of these nanoparticles have been widely used in different works without any toxic effects.[39,48−50] After 5 days, SOST, Runx2, and Alp mRNA were measured by qRT-PCR (Figure 10). Because the injection of the nanoparticles was local, *i.e.*, the nanoparticles were already at the target tissue, we did not evaluate the biodistribution of the nanoparticles in the animals.

First, it should be mentioned that, the expression of SOST in ovariectomized mice (OVX) increased compared to non-ovariectomized mice (control) and were statistically significant. However, the injection of the nanoparticles, with SOST siRNA or osteostatin notably decreased the expression of SOST (*ca.* 50% and 60%, respectively), being particularly effective the injection of the SOST siRNA and osteostatin coloaded nanoparticles, which achieved the greatest knockdown effect, *ca.* 75% of silencing (Figure 10B).

The osteogenic markers, Runx2 and Alp, decreased their expression in OVX compared to Control group as expected (Figure 10C,D). The results also showed that Runx2 and Alp expression notably increased when osteostatin and SOST siRNA were released together by the complete system (up to 3 or 2.2 *n*-fold, respectively, compared with OVX), in total agreement with the previously *in vitro* results. The results obtained with the administration of the system loaded just with the SOST siRNA (OVX+MSNs-siRNA) or only with the osteostatin (OVX+MSNs-OST) were also measured, being up to 1.5 or 2.5 *n*-fold, respectively, for Runx2 and up to 1.8 or 2.6 *n*-fold, respectively, for Alp, compared with OVX. The data showed that the co-administration of both biomolecules at the same time compared with the administration of the biomolecules separately, increased the expression of both osteogenic markers to notably higher levels and decreased the expression of SOST gene, being a combined effect between osteostatin and siRNA (OVX plus MSNs-siRNA plus OST).

The design of the dual delivery nanosystem enhanced the expression of osteogenic markers and, effectively, knockdown of the SOST gene through the combined effect of osteostatin and SOST siRNA *in vivo*, being a synergy between this two molecules. This complete system could provide a potential alternative to the current treatment of osteoporosis, empowering cell differentiation by osteogenic features.

CONCLUSIONS

The inhibition of the Wnt/β-catenin pathway has recently gained attention as therapeutic target in bone diseases such as osteoporosis. One of the main inhibitors of this pathway is sclerostin, a protein encoded by the SOST gene. Its activity results in a reduction of osteoblast formation and differentiation. Several types of sclerostin monoclonal antibodies have been developed as anabolic drugs to block the activity of sclerostin, increasing osteoblast differentiation for osteoporosis treatment.[5,9,51−53] However, these antibodies can cause an immune response, which limits the use of this treatment.[53] Silencing SOST gene with a specific siRNA in osteocytes could be a more effective approach that could overcome the immune response limitation. Osteocytes are the most abundant cells in bone tissue and responsible for SOST gene expression. In face of the difficulties with finding an osteocyte *in vitro* model that expresses SOST; we had to use MEFs, which are known to generate detectable levels of SOST expression. We optimized the conditions of MEFs culturing so we could use them as a platform to test the siRNA effectivity. Even though siRNAs seem to be promising candidates as therapy agents for bone disorders, their main problem relies on their delivery due to their very short half-life and poor internalization capacity through cell membranes. This is an old problem for nucleic acid therapeutics, in which the major challenge has remained the same for the last 40 years.[54] Here, we have employed MSNs as siRNA nanocarriers due to their exquisite properties for drug delivery, such as large surface area, high loading capacity, and biocompatibility, among others. We took advantage of the network of cavities within of MSNs to load the pores with the osteogenic peptide osteostatin, which has been observed to stimulate osteoblastic cell growth and differentiation.

Hence, our purpose was to co-deliver two therapeutic agents, SOST siRNA and osteostatin, at the same time inside cells. After evaluation of the effect of both biomolecules *in vitro* with promising results (high capacity of silencing SOST and notably higher levels of the osteogenic markers), the system was injected in the femoral bone marrow of ovariectomized mice, and the obtained results were in agreement with the *in vitro* experiments. However, mice treated with each biomolecule separately have modified the expression of the three genes, (knocking down SOST and increasing the expression of Runx2 and Alp), the co-administration of both biomolecules yielded synergistic effects. Thus, it can be concluded that our system was able to transport, co-deliver, and transfect to cells SOST siRNA and osteostatin, maintaining its activity and achieving an effective silencing effect. The combination of SOST siRNA with the osteogenic peptide, promoted a synergistic effect, thus increasing the expression of early markers of osteogenic differentiation in ovariectomized mice. These promising results might lead to further investigations. This system has demonstrated remarkable efficacy for an intrabone marrow injection. In consequence, this system will constitute a promising candidate as a platform for gene therapy in osteoporosis treatment.

METHODS

Synthesis and Surface Modification of Mesoporous Silica Nanoparticles. Mesoporous silica nanoparticles, MSNs, were synthesized following a modification of the Stöber method.[43] First, cetyltrimethylammonium bromide (CTAB (1 g, 2.74 mmol)), the structure directing agent, was dissolved in H_2O (480 mL) and NaOH (3.5 mL, 2 M) in a 1 L round-bottom flask under moderate magnetic stirring. The mixture was heated at 80 °C, and tetraethylorthosilicate (TEOS (4.5 mL, 20.15 mmol)) was added drop-wise at 0.33 mL/min rate with a pump. For the phosphonate modification, 30 min after the TEOS addition, 3-trihydroxysilylpropyl methylphosphonate (TSPMP (0.5 mL, 1.31 mmol)) was added and heated for a further 1.5 h at 80 °C under magnetic stirring. Then, the solution was centrifuged and washed once with water and twice with ethanol. The product was

DOI: 10.1021/acsnano.9b00241
ACS Nano 2019, 13, 5451−5464

dried at room temperature under vacuum. The surfactant was removed by ionic exchange using 350 mL of a solution of ammonium nitrate (10 mg/mL) in ethanol (95%) at 80 °C overnight under magnetic stirring. The product was centrifuged, washed 3 times with ethanol, and dried under vacuum.

Rhodamine B-labeled nanoparticles and fluorescein isothiocyanate (FITC)-labeled nanoparticles were synthesized by reacting 1 mg of Rhodamine-B isothiocyanate or fluorescein isothiocyanate with 2.2 μL of (3-aminopropyl)triethoxysilane (APTES) in 100 μL of ethanol for 2 h. Then, this solution was mixed with 4.5 mL of TEOS, and the whole mixture was added to the surfactant solution as previously described. The rest of the procedure was carried out as described above.

For the synthesis of cyanine-7-labeled nanoparticles, 5 mg of cyanine-7 with 4.4 μL of APTES were dissolved in 140 μL of dimethyl sulfoxide and stirred overnight. Then, this solution was mixed with 4.5 mL of TEOS, and the whole mixture was added to the surfactant solution as previously described. The rest of the procedure was carried out as described above.

To perform the PEI coating, 5 mg of phosphonate-modified nanoparticles were dispersed in a solution of 2.5 mg of PEI (5, 8, and 10 kDa) in 1 mL of absolute ethanol. After sonicating for 20 s and stirring for 30 min, the PEI coated nanoparticles (MSNs@PEI) were consequently washed with PBS and ethanol.[41]

Physicochemical Characterization of MSNs. All of the materials were characterized for size, shape, and charge. Surface morphology was analyzed by transmission electron microscopy (TEM) carried out with a JEOL JEM 2100 instrument operated at 200 kV, equipped with a charge-coupled device camera (KeenView Camera). The ζ potential and hydrodynamic size of nanoparticles were measured by means of a Zetasizer Nano ZS (Malvern Instruments) equipped with a 633 nm "red" laser. The PEI coating was verified by thermogravimetry and Fourier-transform infrared (FTIR) spectra. Thermogravimetry and differential temperature analyses (TGA/DTA) were performed in a PerkinElmer Pyris Diamond TG/DTA analyzer, with 5 °C/min heating ramping up from room temperature to 600 °C. A Nicolet Nexus spectrometer (Thermo Fisher Scientific) was used to obtain the FTIR spectra. X-ray diffraction (XRD) was carried out to confirm the order of the mesopores from the nanoparticles in a Philips X-Pert MPD diffractometer equipped with Cu Kα radiation. N_2 adsorption was carried out to obtain surface area and pore size values. Micromeritics ASAP 2010 instrument was used; surface area was obtained by applying the BET method to the isotherm, and the pore size distribution was determined by the BJH method from the desorption branch of the isotherm. The mesopore diameter was determined from the maximum of the pore size distribution curve. Fluorescence spectrometry was used to determine cargo release by means of a Biotek Synergy 4 device. Fluorescence microscopy was used to verify the colocalization on MSNs and siRNA constructs. It was performed with an Evos FL Cell Imaging System equipped with three LED light cubes (lEX, nanometers; lEM, nanometers): DAPY (357/44; 447/60), GFP (470/22; 525/50), and RFP (531/40; 593/40) from AMG (Advance Microscopy Group).

Optimization of siGLO Binding to MSNs@PEI Nanoparticles. The transfection conditions and the release efficiency were optimized using a siRNA-analog called siGLO Green Transfection Indicator (Abs/Em max 494/520 nm). The siRNA binding capability of MSNs@PEI was determined by agarose gel retardation assay. Different amounts of MSNs@PEI ranging from 0.8 to 6.4 μg were mixed with 0.1 μg of siGLO in aqueous solution to obtain particle-to-nucleic acid ratios (N/P) of 8−64. N/P is a mass ratio in which N and P, respectively, correspond to the moles of positive (nitrogen (MSNs@PEI)) and negative (phosphonate (siGLO)) charges. Free siGLO was used as control. A total of 20 μL of MSNs@PEI and siGLO complex solution were mixed with 5 μL of loading buffer and electrophoresed in a 2% agarose gel containing 0.5 μg/mL of GelRed (Nucleic Acid Gel Stain) at 80 V for 40 min in Tris/Borate/EDTA (TBE) running buffer. Nucleic acid bands were detected by UV light (254 nm). It is important to mention that only uncomplexed siGLO is able to migrate to the positive electrode and, therefore, observed on the gel. Then, when the spot of free siGLO is no longer visible means that the amount of nanoparticles added had complexed with all the siGLO present (total binding particle/nucleic acid). The lowest N/P ratio that complexed all the siGLO is called threshold.[41] In 8 and 10 kDa MSN@PEI appears the same threshold, 32, but for 5 kDa PEI, the threshold was 16.

SiGLO Loading and Release from MSNs@PEI. The final concentration to bind the siGLO in the polymer (N/P ratio of 32) was achieved adding 165 μL of siGLO (20 μM) to 0.35 mL of a 4 mg/mL solution of MSNs@PEI in PBS 7.4 (10 mM). A 24-transwell plate was employed to determine the siGLO release. To perform the assay, 0.1 mL of the nanoparticle dispersion were placed on a Transwell permeable support (three replications were performed). The well was filled with 0.6 mL of PBS pH 7.4 (10 mM), and the suspension was orbitally stirred at 37 °C at 100 rpm during all the experiment. At every time point studied, the solution outside the transwell insert was removed and replaced with fresh PBS. The amount of cargo released in the solution removed was determined by fluorescence (absorbance/emission: 494/520 nm).

Cell Cultures. Cell culture tests were performed using MEFs because they are known to express SOST gene. MEF cells were then plated at a density of 20 000 cells per square centimeter in 1 mL of DMEM, respectively, containing 10% of heat-inactivated fetal bovine serum and 1% penicillin−streptomycin at 37 °C in a humidified atmosphere of 5% CO_2, and incubated for the specific time of each experiment. The tested nanoparticles were placed into each well of 12- or 24-well plates after cell seeding. Some wells without nanoparticles were seeded as controls.

Cell Viability. MEF viability was determined by addition of Alamar Blue solution at 10% (v/v) to the cell culture. After 2 h of contact with different concentrations of modified MSNs (n = 3), the cells were grown for 48 h in 24 well plates at a density of 10^4 cells per square centimeter. Afterward, Alamar Blue solution was added following the manufacturer's instructions.[55] Fluorescence intensity was measured using excitation emission wavelengths of 570 and 600 nm, respectively, in a Unicam UV-500 UV−visible spectrophotometer.

Cell MSNs@PEI Uptake by Flow Cytometry, Fluorescence, and Confocal Laser Scanning Microscopy. MEF cells were cultured in each well of a 12-well plate and incubated at different times in the absence or presence of the tested FITC-labeled nanoparticles at a concentration of 50 μg/mL (MSNs, MSNs@PEI, and MSNs@PEI-siGLO). After 2 h, cells were washed twice with PBS and incubated at 37 °C with trypsin−EDTA solution for cell detachment. The reaction was stopped with culture medium after 5 min, and cells were centrifuged at 1000 rpm for 10 min and suspended in fresh medium. Then, the fluorescence present in the surface of the cells was quenched with Trypan blue (0.4%) to confirm the presence of intracellular and, therefore, internalized fluorescent signal. Flow cytometry measurements were performed at an excitation wavelength of 488 nm, and green fluorescence was measured at 530 nm (FL1). The trigger was set for the green fluorescence channel (FL1). The conditions for the data acquisition and analysis were established using negative and positive controls with the CellQuest Program of Becton−Dickinson, and these conditions were maintained during all the experiments. Each experiment was carried out three times and single representative experiments are displayed. For statistical significance, at least 10 000 cells were analyzed in each sample in a FACScan machine (Becton, Dickinson and Company) and the mean of the fluorescence emitted by these single cells was used.

The cell uptake of MSNs was evaluated using fluorescence and confocal laser scanning microscopy incubating the cells with Rhodamine-B-labeled MSNs, MSNs@PEI, and MSNs@PEI-siGLO for 2 h. Each well was washed with PBS three times to clear the no internalized nanoparticles and then fixed with 75% ethanol for 10 min. Cells were permeabilized with 0.5% of Triton X-100 during 5 min. The nonspecific background was reduced through the addition of 1% bovine serum albumin (BSA) to the solution and left for 20 min. The

DOI: 10.1021/acsnano.9b00241
ACS Nano 2019, 13, 5451−5464

nucleus of both types of cells were stained with 4′,6-diamidino-2-fenilindol (DAPI, ≥ 98%) for 5 min, respectively, and then washed three times with PBS. The nanoparticles internalized into MEF cells were evaluated by fluorescence microscopy and performed with an Evos FL Cell Imaging System and with a confocal laser scanning microscope Olympus FV1200. The images were prepared for analysis using 3D Imaris software to project a single 2D image from the multiple Z sections by using an algorithm that displays the maximum value of the pixel of each Z slice of 1 μm of depth. The resulting projection was then converted into an image file using this software. The red channel was used for detecting Rhodamine-B-labeled MSNs@PEI, green channel for siGLO and blue for cell nucleus.

SOST mRNA Expression and siRNA Transfection. MEFs were seeded in 12-well plates and incubated during 3, 7, 14, and 21 days (n = 3). Total RNA was isolated from MEF cells by a standard procedure (Trizol, Invitrogen, Groningen, The Netherlands), and cDNA synthesis was performed using a high-capacity RNA-to-cDNA kit. Gene expression was analyzed by real-time PCR using a QuantStudio 5 Real-Time PCR System. Unlabeled mouse-specific primers for SOST, Runx2, Alp, and TaqMan ^{MGB} probe were used to perform qRT-PCR assay. The mRNA copy numbers were calculated for each sample by using the cycle threshold (Ct) value. Glyceraldehyde 3-phosphate dehydrogenase (GAPDH) rRNA (a housekeeping gene) was amplified in parallel with tested genes. The relative gene expression was represented by $2-\Delta\Delta Ct$, where $\Delta\Delta Ct = \Delta Ct_{target\ gene} - \Delta Ct_{GAPDH}$.

The efficacy of gene silencing using specific SOST siRNA on MEFs *in vitro* was tested seeding cells in 12-well plates and incubated for 2 weeks. Cells were then transfected with the specific siRNAs at 0.5 μM concentration and incubated as required (experiments run for triplicate). To optimize the experiment, two controls were used: a negative control siRNA ("non-targeting control", which targets a site that is absent in human, mouse, and rat genomes) as well as a positive control ("GAPD control", which targets GAPDH, a gene common between human, mouse, and rat). SiRNA transfection was promoted using Accell siRNA transfection media. Transfection progressed for 2 h and after that, and cells were lysed with 500 μL of Trizol. Then, gene expression was analyzed by real-time PCR as described before. Bar graphs represent expression of SOST mRNA relative to GAPDH.

SOST mRNA Knockdown by MSNs@PEI-siRNA. MSNs@PEI-siRNA complexes were prepared with the N/P ratios previously described. First, 15 μL of 20 μM SOST siRNA or negative or positive control siRNA were added to 70 μg of MSNs@PEI 5kD (N/P ratio = 16) in 600 μL of DMEM. The complexes were added to MEFs cells at day 14 and exposed for 2 h. Then, the medium was replaced with fresh medium and cultured for further 48 h. Cells were then lysed using 500 μL of Trizol, and the SOST, Runx2, and Alp expression levels were quantified by real-time PCR as previously described.

Osteostatin Loading and Release. The MSNs were loaded before PEI coating with osteostatin (OST) by incubating 5 mg of MSNs in a solution of OST 10^{-4} M in PBS overnight at 4 °C to maintain osteostatin stability. Then, the nanoparticles were recovered by centrifugation and washed with PBS. The loaded nanoparticles were functionalized with PEI, as previously described. Then, the OST-loaded MSNs@PEI nanoparticles (OST-MSNs@PEI) were centrifuged and washed with PBS.

A 24-transwell plate was employed to determine the OST release. From a 14 mg/mL dispersion of OST-MSNs@PEI dispersed in PBS with a pH of 7.4 (10 mM), 0.1 mL was placed on a Transwell permeable support (3 replications were performed). The well was filled with 0.6 mL of PBS pH 7.4 (10 mM), and the suspension was stirred at 100 rpm at 37 °C during the experiment. At every time point studied, the solution outside the transwell insert was measured by fluorescence and replaced again on the plate. The amount of cargo released was determined by fluorescence at a wavelength of absorbance/emission of 280/320 nm. It was confirmed by a gel electrophoresis assay that osteostatin loading process keeps unaffected the binding ability of OST-MSNs@PEI to siGLO.

Osteostatin Delivery in MEF Cells in the Presence and Absence of siRNA SOST. For the performance of the experiment, first MSNs were loaded with osteostatin as described before; afterward, they were coated with PEI and bound to siRNA (OST-MSNs@PEI-siRNA). Then, 15 μL of 20 μM SOST siRNA or negative or positive control siRNA were added to 70 μg of OST-MSNs@PEI 5kD (N/P ratio of 16) in 600 μL of DMEM. The complexes were added to MEFs cells at day 14 and exposed for 2 h. OST-MSNs@PEI were also used as control. Then, the medium was replaced with fresh medium and cultured for further 48 h. Cells were then lysed using 500 μL of Trizol, and the SOST, Runx2, and Alp expression levels were quantified by real-time PCR as previously described.

***In Vivo* Evaluation.** Young mature virgin female C57BL/6J mice (Charles River) that underwent bilateral OVX or sham operations (control) of 12 weeks of age were used. They were assigned to 6 groups (n = 5 per group), OVX, MSNs, MSNs@PEI-siCtl, MSNs@PEI-siRNA, OST-MSNs@PEI, OST-MSNs@PEI-siRNA, and one more control group with 5 mice. They were stabilized in the Animal Research Facility at Hospital 12 de Octubre for 2 weeks. All animal experiments in this study were performed according to approved protocols. Animals were given free access to water and fed a standard diet (8.8 g/kg calcium and 5.9 g/kg phosphate) in a room maintained at 22 °C on 12 h light/12 h dark cycles.

Mice were anesthetized with isoflurane, and 50 μL of nanoparticle dispersion (0.8 mg/mL) was injected in the femur bone marrow by bilateral oblique incisions that were made over the patellar ligament. A hole was made through patellar ligament using the needle from the syringe, and then the dispersion was injected.

After 5 days, mice were euthanized by incubating them with 5% isoflurane in oxygen, and both femurs, the one injected with nanoparticles and the other one as control, were removed. Bone samples were crushed under liquid nitrogen. Total RNA was extracted from these homogenized samples with Trizol following the manufacturer's instructions. SOST, Runx2, and Alp expression levels were quantified by real-time PCR as previously described.

Dual-Energy X-ray Absorptiometry. The bone mineral density of femur was measured in anaesthetized control and ovariectomized mice at the start of the study to confirm decreased bone mass using PIXImus (GE Lunar Corp., Madison, WI).[12]

ASSOCIATED CONTENT

Supporting Information

The Supporting Information is available free of charge on the ACS Publications website at DOI: 10.1021/acsnano.9b00241.

Figures showing physicochemical characterizations, MEF cell viability, time-dependent SiGLO release, SOST gene expression knockdown in the presence of SiRNA-Sost in MEF cells, and representative fluorescence microscopy images; tables showing particle size and ζ potential before and after coating with PEI and particle size and size distribution graphics (PDF)

AUTHOR INFORMATION

Corresponding Authors

*E-mail: vallet@ucm.es.
*E-mail: mmanzano@ucm.es.

ORCID

Patricia Mora-Raimundo: 0000-0001-5382-2743
Daniel Lozano: 0000-0001-5902-9201
Miguel Manzano: 0000-0001-6238-6111
María Vallet-Regí: 0000-0002-6104-4889

Notes

The authors declare no competing financial interest.

DOI: 10.1021/acsnano.9b00241
ACS Nano 2019, 13, 5451−5464

ACKNOWLEDGMENTS

This work has been done thanks to the financial support provided by European Research Council (Advanced Grant VERDI; ERC-2015-AdG proposal no. 694160).

REFERENCES

(1) Kanis, J. A.; McCloskey, E. V.; Johansson, H.; Oden, A.; Melton, L. J.; Khaltaev, N. A Reference Standard for the Description of Osteoporosis. *Bone.* **2008**, *42*, 467−475.
(2) Kanis, J. A. Assessment of Fracture Risk and Its Application to Screening for Postmenopausal Osteoporosis: Synopsis of a WHO Report. *Osteoporosis Int.* **1994**, *4*, 368−381.
(3) Moshiri, A.; Sharifi, A. M.; Oryan, A. Current Knowledge, Drug-Based Therapeutic Options and Future Directions in Managing Osteoporosis. *Clin. Rev. Bone Miner. Metab.* **2017**, *15*, 1−23.
(4) Arcos, D.; Boccaccini, A. R.; Bohner, M.; Díez-Pérez, A.; Epple, M.; Gómez-Barrena, E.; Herrera, A.; Planell, J. A.; Rodríguez-Mañas, L.; Vallet-Regí, M. The Relevance of Biomaterials to the Prevention and Treatment of Osteoporosis. *Acta Biomater.* **2014**, *10*, 1793−1805.
(5) Khajuria, D. K.; Razdan, R.; Mahapatra, D. R. Drugs for the Management of Osteoporosis: A Review. *Rev. Bras. Reumatol.* **2011**, *51*, 372−382.
(6) Rachner, T. D.; Khosla, S.; Hofbauer, L. C. Osteoporosis: Now and the Future. *Lancet* **2011**, *377*, 1276−1287.
(7) Russell, R. G. G. Bisphosphonates: The First 40 Years. *Bone.* **2011**, *49*, 2−19.
(8) Mackey, P. A.; Whitaker, M. D. Osteoporosis: A Therapeutic Update. *J. Nurse Pract.* **2015**, *11*, 1011−1017.
(9) Iñiguez-Ariza, N. M.; Clarke, B. L. Bone Biology, Signaling Pathways, and Therapeutic Targets for Osteoporosis. *Maturitas* **2015**, *82*, 245−255.
(10) Esbrit, P.; Herrera, S.; Portal-Núñez, S.; Nogués, X.; Díez-Pérez, A. Parathyroid Hormone-Related Protein Analogs as Osteoporosis Therapies Therapy. *Calcif. Tissue Int.* **2016**, *98*, 359−369.
(11) Cornish, J.; Callon, K. E.; Lin, C.; Xiao, C.; Moseley, J. M.; Reid, I. A. N. R. Stimulation of Osteoblast Proliferation by C-Terminal Fragments of Parathyroid Hormone - Related Protein. *J. Bone Miner. Res.* **1999**, *14*, 915−922.
(12) Lozano, D.; Fernández-De-Castro, L.; Portal-Núñez, S.; López-Herradón, A.; Dapía, S.; Gómez-Barrena, E.; Esbrit, P. The C-Terminal Fragment of Parathyroid Hormone-Related Peptide Promotes Bone Formation in Diabetic Mice with Low-Turnover Osteopaenia. *Br. J. Pharmacol.* **2011**, *162*, 1424−1438.
(13) Fenton, A. J.; Kemp, B. E.; Kent, G. N.; Moseley, J. M.; Zheng, M.; Rowe, D. J.; Britto, J. M.; Martin, T. J.; Nicholson, G. C. A Carboxyl-Terminal Peptide from the Parathyroid Hormone-Related Protein Inhibits Bone Resorption by Osteoclasts. *Endocrinology* **1991**, *129*, 1762−1768.
(14) Lewinson, D.; Rihani-Basharat, S. Rapid Communication PTHrP (107 - 111) Inhibits *In Vivo* Resorption That Was Stimulated by PTHrP (1 - 34) When Applied Intermittently to Neonatal Mice. *Calcif. Tissue Int.* **1997**, *61*, 426−428.
(15) Lozano, D.; Trejo, C. G.; Gómez-Barrena, E.; Manzano, M.; Doadrio, J. C.; Salinas, A. J.; Vallet-Regí, M.; García-Honduvilla, N.; Esbrit, P.; Buján, J. Osteostatin-Loaded onto Mesoporous Ceramics Improves the Early Phase of Bone Regeneration in a Rabbit Osteopenia Model. *Acta Biomater.* **2012**, *8*, 2317−2323.
(16) Lozano, D.; Sánchez-Salcedo, S.; Portal-Núñez, S.; Vila, M.; López-Herradón, A.; Ardura, J. A.; Mulero, F.; Gómez-Barrena, E.; Vallet-Regí, M.; Esbrit, P. Parathyroid Hormone-Related Protein (107−111) Improves the Bone Regeneration Potential of Gelatin - Glutaraldehyde Biopolymer-Coated Hydroxyapatite. *Acta Biomater.* **2014**, *10*, 3307−3316.
(17) Lozano, D.; Manzano, M.; Salinas, A. J.; Esbrit, P.; Doadrio, J. C.; Vallet-Regí, M.; Gómez-Barrena, E. Osteostatin-Loaded Bioceramics Stimulate Osteoblastic Growth and Differentiation. *Acta Biomater.* **2010**, *6*, 797−803.
(18) Tokatlian, T.; Segura, T. siRNA Applications in Nanomedicine. *WIREs Nanomed Nanobiotechnol.* **2010**, *2*, 305−315.
(19) Zhang, G.; Guo, B.; Wu, H.; Tang, T.; Zhang, B.-T.; Zheng, L.; He, Y.; Yang, Z.; Pan, X.; Chow, H.; et al. A Delivery System Targeting Bone Formation Surfaces to Facilitate RNAi-Based Anabolic Therapy. *Nat. Med.* **2012**, *18*, 307−314.
(20) Kim, T.; Singh, R. K.; Kang, M. S.; Kim, J.; Kim, H. Inhibition of Osteoclastogenesis through siRNA Delivery with Tunable Mesoporous Bioactive Nanocarriers. *Acta Biomater.* **2016**, *29*, 352−364.
(21) Wang, Y.; Tran, K. K.; Shen, H.; Grainger, D. W. Selective Local Delivery of RANK siRNA to Bone Phagocytes Using Bone Augmentation Biomaterials. *Biomaterials* **2012**, *33*, 8540−8547.
(22) Sun, Y.; Ye, X.; Cai, M.; Liu, X.; Xiao, J.; Zhang, C.; Wang, Y.; Yang, L.; Liu, J.; Li, S.; Kang, C.; Zhang, B.; Zhang, Q.; Wang, Z.; Hong, A.; Wang, X. Osteoblast-Targeting-Peptide Modified Nanoparticle for siRNA/microRNA Delivery. *ACS Nano* **2016**, *10*, 5759−5768.
(23) Baron, R.; Kneissel, M. WNT Signaling in Bone Homeostasis and Disease: From Human Mutations to Treatments. *Nat. Med.* **2013**, *19*, 179−192.
(24) Duan, P.; Bonewald, L. F. The Role of the Wnt/β-Catenin Signaling Pathway in Formation and Maintenance of Bone and Teeth. *Int. J. Biochem. Cell Biol.* **2016**, *77*, 23−29.
(25) Wang, Y.; Li, Y.-P.; Paulson, C.; Shao, J.-Z.; Zhang, X.; Wu, M.; Chen, W. Wnt and the Wnt Signaling Pathway in Bone Development and Disease. *Front. Biosci., Landmark Ed.* **2014**, *19*, 379−407.
(26) Pietrzyk, B.; Smertka, M.; Chudek, J. Sclerostin: Intracellular Mechanisms of Action and Its Role in the Pathogenesis of Skeletal and Vascular Disorders. *Adv. Clin. Exp. Med.* **2017**, *26*, 1283−1291.
(27) Zhang, J.; Li, X.; Huang, L. Non-Viral Nanocarriers for siRNA Delivery in Breast Cancer. *J. Controlled Release* **2014**, *190*, 440−450.
(28) Basha, G.; Ordobadi, M.; Scott, W. R.; Cottle, A.; Liu, Y.; Wang, H.; Cullis, P. R. Lipid Nanoparticle Delivery of siRNA to Osteocytes Leads to Effective Silencing of SOST and Inhibition of Sclerostin *in Vivo*. *Mol. Ther.–Nucleic Acids* **2016**, *5*, 1−15.
(29) Cavallaro, G.; Sardo, C.; Craparo, E. F.; Porsio, B.; Giammona, G. Polymeric Nanoparticles for siRNA Delivery: Production and Applications. *Int. J. Pharm.* **2017**, *525*, 313−333.
(30) Goyal, R.; Tripathi, S. K.; Tyagi, S.; Sharma, A.; Ram, K. R.; Chowdhuri, D. K.; Shukla, Y.; Kumar, P.; Gupta, K. C. Linear PEI Nanoparticles: Efficient pDNA/siRNA Carriers *in Vitro* and *in Vivo*. *Nanomedicine (N. Y., NY, U. S.)* **2012**, *8*, 167−175.
(31) Swami, A.; Kurupati, R. K.; Pathak, A.; Singh, Y.; Kumar, P.; Gupta, K. C. *Biochem. Biophys. Res. Commun.* **2007**, *362*, 835−841.
(32) Manzano, M.; Vallet-Regí, M. Mesoporous Silica Nanoparticles in Nanomedicine Applications. *J. Mater. Sci.: Mater. Med.* **2018**, *29*, 65.
(33) Mora-Raimundo, P.; Manzano, M.; Vallet-Regí, M. Nanoparticles for the Treatment of Osteoporosis. *AIMS Bioeng.* **2017**, *4*, 259−274.
(34) Vallet-Regí, M.; Balas, F.; Arcos, D. Mesoporous Materials for Drug Delivery. *Angew. Chem., Int. Ed.* **2007**, *46*, 7548−7558.
(35) Vallet-Regí, M.; Rámila, A.; Del Real, R. P.; Pérez-Pariente, J. A New Property of MCM-41: Drug Delivery System. *Chem. Mater.* **2001**, *13*, 308−311.
(36) Villaverde, G.; Nairi, V.; Baeza, A.; Vallet-Regí, M. Double Sequential Encrypted Targeting Sequence: A New Concept for Bone Cancer Treatment. *Chem. - Eur. J.* **2017**, *23*, 7174−7179.
(37) Baeza, A.; Noureddine, A.; Durfee, P. N.; Butler, K. S.; Agola, J. O.; Villegas, M. R.; Brinker, C. J.; Vallet-Regi, M. Multifunctional Protocells for Enhanced Penetration in 3D Extracellular Tumoral Matrices. *Chem. Mater.* **2018**, *30*, 112−120.
(38) Gisbert-Garzarán, M.; Lozano, D.; Vallet-Regí, M.; Manzano, M. Self-Immolative Polymers as Novel pH-Responsive Gate Keepers for Drug Delivery. *RSC Adv.* **2017**, *7*, 132−136.
(39) Paris, J. L.; Cabañas, M. V.; Manzano, M.; Vallet-Regí, M. Polymer-Grafted Mesoporous Silica Nanoparticles as Ultrasound-Responsive Drug Carriers. *ACS Nano* **2015**, *9*, 11023−11033.

DOI: 10.1021/acsnano.9b00241
ACS Nano 2019, 13, 5451−5464

(40) Hom, C.; Lu, J.; Liong, M.; Luo, H.; Li, Z.; Zink, J. I.; Tamanoi, F. Mesoporous Silica Nanoparticles Facilitate Delivery of siRNA to Shutdown Signaling Pathways in Mammalian Cells. *Small* **2010**, *6*, 1185−1190.
(41) Meng, H.; Liong, M.; Xia, T.; Li, Z.; Ji, Z.; Zink, J. I.; Nel, A. E. Engineered Design of Mesoporous Silica Nanoparticles to Deliver Doxorubicin and Pgp siRNA to Overcome Drug Resistance in a Cancer Cell Line. *ACS Nano* **2010**, *4*, 4539−4550.
(42) Trejo, C. G.; Lozano, D.; Manzano, M.; Doadrio, J. C.; Salinas, A. J.; Dapía, S.; Gómez-Barrena, E.; Vallet-Regí, M.; García-Honduvilla, N.; Buján, J. The Osteoinductive Properties of Mesoporous Silicate Coated with Osteostatin in a Rabbit Femur Cavity Defect Model. *Biomaterials* **2010**, *31*, 8564−8573.
(43) Stober, W.; Fink, A.; Bohn, E. Controlled Growth of Monodispersed Silica Spheres in the Micron Size Range. *J. Colloid Interface Sci.* **1968**, *26*, 62−69.
(44) Xia, T.; Kovochich, M.; Liong, M.; Meng, H.; Kabehie, S.; George, S.; Zink, J. I.; Nel, A. E. Polyethyleneimine Coating Enhances the Cellular Uptake of Mesoporous Silica Nanoparticles and Allows Safe Delivery of siRNA and DNA Constructs. *ACS Nano* **2009**, *3*, 3273−3286.
(45) Fuller, J. E.; Zugates, G. T.; Ferreira, L. S.; Ow, H. S.; Nguyen, N. N.; Wiesner, U. B.; Langer, R. S. Intracellular Delivery of Core-Shell Fluorescent Silica Nanoparticles. *Biomaterials* **2008**, *29*, 1526−1532.
(46) Lozano, D.; Feito, M. J.; Portal-Núñez, S.; Lozano, R. M.; Matesanz, M. C.; Serrano, M. C.; Vallet-Regí, M.; Portolés, M. T.; Esbrit, P. Osteostatin Improves the Osteogenic Activity of Fibroblast Growth Factor-2 Immobilized in Si-Doped Hydroxyapatite in Osteoblastic Cells. *Acta Biomater.* **2012**, *8*, 2770−2777.
(47) de Castro, L. F.; Lozano, D.; Portal-Núñez, S.; Maycas, M.; de la Fuente, M.; Caeiro, J. R.; Esbrit, P. Comparison of the Skeletal Effects Induced by Daily Administration of PTHrP (1−36) and PTHrP (107−139) to Ovariectomized Mice. *J. Cell. Physiol.* **2012**, *227*, 1752−1760.
(48) Dogra, P.; Adolphi, N. L.; Wang, Z.; Lin, Y. S.; Butler, K. S.; Durfee, P. N.; Croissant, J. G.; Noureddine, A.; Coker, E. N.; Bearer, E. L.; Cristini, V.; Brinker, C. J. Establishing the Effects of Mesoporous Silica Nanoparticle Properties on *in Vivo* Disposition Using Imaging-Based Pharmacokinetics. *Nat. Commun.* **2018**, *9*, 1−14.
(49) Wen, S.; Zheng, F.; Shen, M.; Shi, X. Surface Modification and PEGylation of Branched Polyethyleneimine for Improved Biocompatibility. *J. Appl. Polym. Sci.* **2013**, *128*, 3807−3813.
(50) Zink, J. I.; Wang, X.; Ji, Z.; Lin, S.; Xue, M.; Xia, T.; Zhao, Y.; Zhang, H.; Mai, W. X.; Nel, A. E.; Meng, H. Codelivery of an Optimal Drug/siRNA Combination Using Mesoporous Silica Nanoparticles To Overcome Drug Resistance in Breast Cancer *in Vitro* and *in Vivo*. *ACS Nano* **2013**, *7*, 994−1005.
(51) Suen, P. K.; Qin, L. Sclerostin, an Emerging Therapeutic Target for Treating Osteoporosis and Osteoporotic Fracture: A General Review. *J. Orthop. Transl.* **2016**, *4*, 1−13.
(52) Deal, C. Potential New Drug Targets for Osteoporosis. *Nat. Clin. Pract. Rheumatol.* **2009**, *5*, 20−27.
(53) Li, X.; Warmington, K. S.; Niu, Q. T. T.; Asuncion, F. J.; Barrero, M.; Grisanti, M.; Dwyer, D.; Stouch, B.; Thway, T. M.; Stolina, M.; Ominsky, M. S.; Kostenuik, P. J.; Simonet, W. S.; Paszty, C.; Ke, H. Z. Inhibition of Sclerostin by Monoclonal Antibody Increases Bone Formation, Bone Mass, and Bone Strength in Aged Male Rats. *J. Bone Miner. Res.* **2010**, *25*, 2647−2656.
(54) Dowdy, S. F.; Levy, M. RNA Therapeutics (Almost) Comes of Age: Targeting, Delivery and Endosomal Escape. *Nucleic Acid Ther.* **2018**, *28*, 107−108.
(55) Invitrogen. Alamar Blue Assay. U.S. Patent No. 5501959, 5, 1−27.

DOI: 10.1021/acsnano.9b00241
ACS Nano 2019, 13, 5451−5464